Error analysis of spectral estimates with application to the measurement of acoustic parameters using random sound fields in ducts

A. F. Seybert and Benjamin Soenarko[a)]

Department of Mechanical Engineering, University of Kentucky, Lexington, Kentucky 40506
(Received 18 September 1980; accepted for publication 27 October 1980)

Several methods have been proposed using multiple-point pressure measurement of random sound fields in ducts to determine acoustic properties of materials and systems. This paper presents an error analysis of the spectral estimates used in these techniques. Expressions for the normal acoustic absorption coefficient and impedance are derived for a random sound field in a duct. Theory is developed to determine the bias and random errors in estimating the spectral density function for plane-wave propagation in the duct. A bivariate stochastic process has been employed to model the acoustic system. Experimental and theoretical calculations show that minimum-bias error can be achieved by using a small bandwidth in estimating the spectra and by locating the microphones close to the sample. Furthermore, random error can be minimized by maintaining a high coherence between microphone signals. This implies that the microphones should have a small spacing. However, high coherence may not be realized when a microphone location coincides with a node point in the sound field.

PACS numbers: 43.85.Bh, 43.60.Cg, 43.20.Mv

LIST OF SYMBOLS

$b[\hat{S}_{11}]$	bias error of $\hat{S}_{11}$
c	speed of sound in still air
cov	covariance
E	expected value
f	frequency
G_1	error contribution function due to magnitude of transfer function
G_2	error contribution function due to phase angle of transfer function
h_{1S}	impulse response between the first microphone and the source
h_{2S}	impulse response between the second microphone and the source
h_{1N}	impulse response between the first microphone and the background noise
h_{2N}	impulse response between the second microphone and the background noise
$H_{1S}, H_{2S}, H_{1N}, H_{2N}$	Fourier transform of $h_{1S}, h_{2S}, h_{1N}, h_{2N}$, respectively
*	complex conjugate
H_{12}	transfer function between first and second microphone
k	wavenumber without flow
k_i	wavenumber in direction of flow
k_r	wavenumber in opposite direction of flow
l	tube length
L	microphone spacing
M	mean flow Mach number
n_d	number of averages
N_0	background noise
p_i	incident wave pressure
p_r	reflected wave pressure
p_1	total pressure at point 1
p_2	total pressure at point 2
P_i	Fourier transform of incident wave
P_r	Fourier transform of reflected wave
P_1	Fourier transform of total acoustic pressure at point 1
P_2	Fourier transform of total acoustic pressure at point 2
r_p	acoustic pressure reflection coefficient
R_l', Y_l'	normalized resistance and reactance, respectively, at $x=-l$
R_0', Y_0'	normalized resistance and reactance, respectively, at $x=0$
S	tube cross-sectional area
S_{AA}	auto-spectral density of the incident wave
S_{BB}	auto-spectral density of the reflected wave
S_{AB}	cross-spectral density between incident and reflected waves
C_{AB}, Q_{AB}	real and imaginary parts of S_{AB}, respectively
$\hat{S}_{11}$	estimate of the pressure auto-spectral density at point 1
$\hat{S}_{12}$	estimate of the pressure cross-spectral density between points 1 and 2
$\hat{C}_{12}, \hat{Q}_{12}$	real and imaginary parts of $\hat{S}_{12}$, respectively
S_0	acoustic source
$S_{\psi\psi}$	auto-spectral density of $\psi(t)$
t	time coordinate
U	Fourier transform of the total particle velocity
U_i	Fourier transform of the particle velocity of the incident wave
U_r	Fourier transform of the particle velocity of the reflected wave
v	mean flow velocity
var	variance
x	spatial coordinate
x_1	position of first microphone
x_2	position of second microphone

a)On leave from the Department of Engineering Science, Bandung Institute of Technology, Bandung, Indonesia.

 0001-4966/81/041190-10$00.80

Z_1	specific acoustic impedance at $x=-l$
Z_0	specific acoustic impedance at $x=0$
Z_1'	normalized specific acoustic impedance at $x=-l$
Z_0'	normalized specific acoustic impedance at $x=0$
α, β	real and imaginary part of P_2/P_1, respectively
α_n	normal acoustic power absorption coefficient
δ	perturbation
Δf	analysis frequency bandwidth
ϵ_α	normalized standard error of α_n
θ	phase angle of S_{AB}
ρ	density
ψ	exciting force
ϕ_{12}	phase angle of H_{12}
γ_{12}^2	coherence function
σ_S^2	variance of the source S_0
σ_N^2	variance of background noise N_0

INTRODUCTION

The standing wave ratio method is a well-known technique in duct acoustics for measuring the acoustic properties of materials. Although it has been chosen as a standard technique, it is time consuming; and various alternative techniques based on plane-wave theory and utilizing two point pressure measurements have been developed. Johnston and Schmidt[1] used two wall-mounted microphones and cross-correlation measurements between the voltage signal of the source and the output signal from each microphone to deduce the acoustic reflection coefficient of a sample. They reported errors which were traced to uncertainty in the determination of phase angles from the correlograms and uncertainty in determining the true location of the loudspeaker source.

A similar method was developed by Seybert and Ross.[2] They used two wall-mounted microphones and a source of random sound. By measuring the auto- and cross-spectral densities between the microphones, they were able to separate the incident and reflected wave spectra and to calculate the acoustic impedance of a sample. Some statistical considerations were discussed which showed that a compromise must be made between the random and bias errors by selecting the analysis bandwidth and the number of ensemble averages used in smoothing the raw spectral estimates.

Blaser and Chung[3] used a transfer function technique to measure acoustic reflection coefficient and transmission loss. They measured the transfer function between two wall-mounted microphones and the transfer function associated with the incident and reflected waves. They also pointed out the existence of an upper frequency limit determined by microphone spacing.

An error analysis is useful in designing and conducting measurement procedures and in establishing confidence intervals for measured data. Except as noted above, Refs. 2 and 3 do not elaborate on statistical errors associated with acoustic property measurement.

Parrott and Smith[4] developed an analysis of random and systematic measurement error for acoustic impedance estimates using the standing wave ratio method. They found that the random measurement errors in pressure minima position and reflection coefficient approximate a normal probability distribution with standard deviation of 0.0096 cm and 0.001, respectively. They concluded that impedance measurements are more sensitive to random and systematic errors in the measurement of pressure minima position than in the reflection coefficient. Rapp[5] found by experiment that the largest error in measuring acoustic properties of materials using multiple microphones and pure tones was due to the phase angle measurement uncertainty. A large error was shown to occur when the phase angle was near zero or π radians.

Bendat[6] developed guidelines for random error in the measurement of coherence functions and other input/output quantities derived from random processes. Some derivations were carried out that show the dependency of the random error on the coherence function between input and output. He also showed that the bias error in spectral estimates for a second order system is maximum at the resonant frequency.

This paper is intended to investigate random and bias errors in estimating pressure spectra, and quantities derived from pressure spectra, in ducts containing plane-wave sound fields with random intensity variations.

I. RANDOM EXCITATION TECHNIQUE USING TWO MICROPHONES

Consider a duct acoustic system terminated at $x=0$ by an unknown sample, whose specific acoustic impedance is Z_0, and terminated at $x=-l$ by a randomly vibrating piston as shown in Fig. 1. The acoustic pressure is measured at points 1 and 2. In this system, the vibration of the piston is assumed to be stationary with time.

Considering plane-wave propagation along the x axis, the wave equation is

$$\frac{\partial^2 p}{\partial t^2} = c^2 \frac{\partial^2 p}{\partial x^2}, \tag{1}$$

where c is the speed of sound. Let p be represented by a Fourier integral[7]

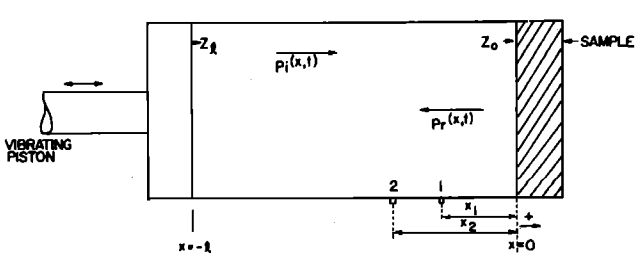

FIG. 1. Duct acoustic system depicting the unknown sample and an acoustic signal source as a randomly vibrating piston.

$$p(x,t) = \int_{-\infty}^{\infty} P(x,f)e^{j2\pi ft}\,df, \tag{2}$$

where $P(x,f)$ is the Fourier transform of $p(x,t)$. Inserting Eq. (2) in Eq. (1) yields:

$$P''(x,f) + k^2P(x,f) = 0,$$

where $k = 2\pi f/c$ is the wavenumber and $P''(x,f)$ is the second derivative of $P(x,f)$ with respect to x. This equation leads to solutions: $P_i(x,f) = A(f)e^{-jk_ix}$ and $P_r(x,f) = B(f)e^{+jk_rx}$, where the subscripts i and r refer to the incident and reflected waves, respectively. When flow is present with Mach number M, $k_i = k/(1+M)$ and $k_r = k/(1-M)$. Therefore the general solution is $P(x,f) = A(f)e^{-jk_ix} + B(f)e^{jk_rx}$. Evaluating the pressures at x_1 and x_2, and solving for $A(f)$ and $B(f)$ yields:

$$A(f) = \frac{P_1\exp(jk_rx_2) - P_2\exp(jk_rx_1)}{\exp[j(k_rx_2 - k_ix_1)] - \exp[j(k_rx_1 - k_ix_2)]}, \tag{3}$$

$$B(f) = \frac{P_2\exp(-jk_ix_1) - P_1\exp(-jk_ix_2)}{\exp[j(k_rx_2 - k_ix_1)] - \exp[j(k_rx_1 - k_ix_2)]}, \tag{4}$$

where P_1 and P_2 are simply $P(x_1,f)$ and $P(x_2,f)$.

The acoustic pressure reflection coefficient is defined as

$$r_p = P_r(0,f)/P_i(0,f) = B(f)/A(f). \tag{5}$$

In terms of reflection coefficient, the normalized specific acoustic impedance can be expressed as

$$Z_0' = Z_0/\rho c = (1+r_p)/(1-r_p), \tag{6}$$

where ρ is the density.

Defining $P_2/P_1 = \alpha + j\beta$ and using Eqs. (3)–(6) for the case where $M=0$ yields the real and imaginary part of Z_0' as follows:

$$\mathrm{Re}\,Z_0' = \frac{\beta\sin k(x_1-x_2)}{\cos^2kx_2 - 2\alpha\cos kx_2\cos kx_1 + (\alpha^2+\beta^2)\cos^2kx_1}, \tag{7}$$

$$\mathrm{Im}\,Z_0' = \frac{(\alpha^2+\beta^2)\sin kx_1\cos kx_1 - \alpha\sin k(x_2+x_1) + \sin kx_2\cos kx_2}{\cos^2kx_2 - 2\alpha\cos kx_2\cos kx_1 + (\alpha^2+\beta^2)\cos^2kx_1}. \tag{8}$$

So, given the position of microphones x_1 and x_2, and measured values of α and β, the specific acoustic impedance can be determined using Eqs. (7) and (8).

The acoustic power absorption coefficient can be expressed in terms of the reflection coefficient by the relation

$$\alpha_n = 1 - |r_p|^2. \tag{9}$$

Employing Eqs. (3)–(5) and (9) yields:

$$\alpha_n = \frac{-4\beta\sin kL}{1 + (\alpha^2+\beta^2) - 2\alpha\cos kL - 2\beta\sin kL}, \tag{10}$$

where $L = x_2 - x_1$.

A. Experimental results

The instrumentation and procedures used in the following tests are essentially the same as described in Ref. 2. A schedule 40 PVC pipe approximately 1 m long with a nominal inside diameter of 5.2 cm was used in the tests. This diameter allows plane-wave propagation up to approximately 3800 Hz.[8] A random noise generator and an amplifer were used to supply voltage to an acoustic driver mounted at one end of the pipe. Two microphones with an axial spacing of approximately 5 cm sensed the pressure in the tube. The ratio P_2/P_1 was determined by the equivalent ratio $\hat{S}_{12}(f)/\hat{S}_{11}(f)$, where $\hat{S}_{12}(f)$ is the estimate of the cross spectrum between $p_1(t)$ and $p_2(t)$ and $\hat{S}_{11}(f)$ is the estimate of the auto spectrum of $p_1(t)$. The spectra were obtained by using a two-channel spectrum analyzer and Eq. (10) was evaluated using a desktop computer.

Figure 2 shows the results of measurements of the absorption coefficient of single and double layers of glasswool, where each layer was 0.02 m thick. Comparison was made with the results obtained by using the standing wave ratio technique. It can be seen that a good agreement was achieved between these two techniques. However, there is some variation in the absorption coefficient obtained by the standing wave ratio method even though care was taken to obtain accurate standing wave measurements.

In a second test the reactance of a 20 cm long closed tube was obtained using Eq. (8). These data are shown in Fig. 3 where comparison has been made with the theoretical reactance $= -\cot kl$. Figure 4 shows the behavior of the measured coherence function. The magnitude and phase of the transfer function are depicted in Figs. 5 and 6. It can be shown that the dips in the coherence function correspond to the frequencies where a node coincides with either microphone position. At these frequencies the magnitude of the transfer function approaches zero or infinity and its phase angle approaches $\pi/2$. The coherence at the nodal frequencies will be a minimum when the tube has a rigid termination.

II. BIAS ERRORS IN SPECTRAL ESTIMATES

The ratio $\hat{S}_{12}(f)/\hat{S}_{11}(f)$ will be unbiased if $\hat{S}_{12}(f)$ and $\hat{S}_{11}(f)$ are unbiased. The following analysis will illus-

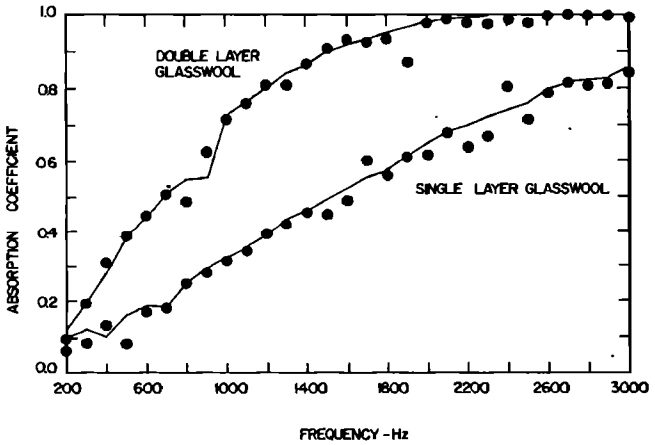

FIG. 2. Measured absorption coefficient of single and double layer glasswool of 0.02 m thick each layer. Solid line: Two microphone method using random excitation; closed circle: SWR method.

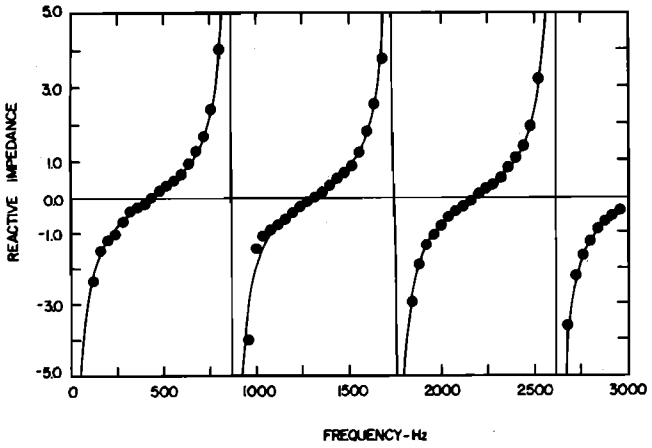

FIG. 3. Impedance of a 20-cm long closed tube. Solid line: Theory; closed circle: Two microphone method using random excitation.

trate the effect of bias errors on these spectral estimates and how bias errors may be avoided.

Suppose the piston in Fig. 1 is driven by a force $\psi(t) = \int_{-\infty}^{\infty} \Psi(f) e^{j2\pi ft}\, df$, where $\Psi(f)$ is the Fourier transform of $\psi(t)$. The length of the tube is l and its cross section is S. The pressure at any point in the tube is composed of the incident and reflected wave pressures. Assuming there is no attenuation in the tube, then for plane-wave propagation the particle velocity is related to the pressure by

$$P_i(x,f) = \rho c U_i(x,f) \quad \text{for the incident wave}, \tag{11}$$

$$P_r(x,f) = -\rho c U_r(x,f) \quad \text{for the reflected wave}. \tag{12}$$

The total pressure at any point in the tube is

$$P(x,f) = A(f)e^{-jkx} + B(f)e^{jkx}, \tag{13}$$

for $M=0$ and $k_i = k_r = k$. Likewise the total particle velocity can be expressed as

$$U(x,f) = [A(f)e^{-jkx} - B(f)e^{jkx}]/\rho c. \tag{14}$$

The boundary conditions are

$$\begin{aligned} &\text{at } x=0;\ Z_0 U(0,f) = P(0,f), \\ &\text{at } x=-l;\ Z_l U(-l,f) + P(-l,f) = \Psi(f)/S, \end{aligned} \tag{15}$$

where Z_l is the specific acoustic impedance of the piston.

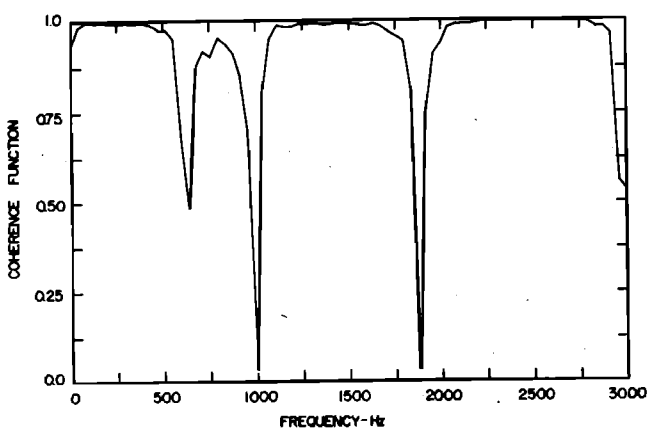

FIG. 4. Measured coherence function between first and second microphone for a closed tube.

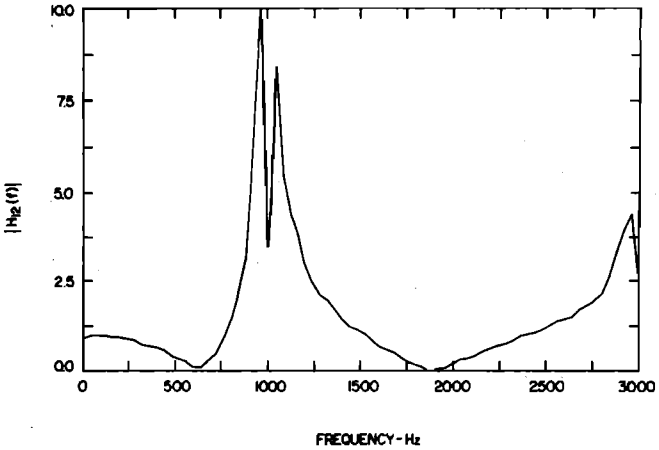

FIG. 5. Magnitude of the transfer function between first and second microphone for a closed tube.

Combining Eqs. (13)–(15) and solving for $A(f)$ and $B(f)$ yields:

$$A(f) = \frac{(Z_0' + 1)}{2S[(Z_l' + Z_0')\cos kl + j(1 + Z_0'Z_l')\sin kl]}\Psi(f), \tag{16}$$

$$B(f) = \frac{(Z_0' - 1)}{2S[(Z_l' + Z_0')\cos kl + j(1 + Z_0'Z_l')\sin kl]}\Psi(f), \tag{17}$$

where $Z_l' = Z_l/\rho c$.

Reference 2 showed that the auto-spectrum of the pressure at any point x is

$$\begin{aligned} S_{11}(f) = {} & S_{AA}(f) + S_{BB}(f) \\ & + 2[C_{AB}(f)\cos 2kx + Q_{AB}(f)\sin 2kx], \end{aligned} \tag{18}$$

where $S_{AA}(f)$ and $S_{BB}(f)$ are the auto-spectral densities of the incident and reflected waves, respectively; $C_{AB}(f)$ and $Q_{AB}(f)$ are the real and imaginary parts of the cross-spectral density $S_{AB}(f)$ between the incident and reflected waves, i.e., $S_{AB}(f) = C_{AB}(f) + jQ_{AB}(f)$. Obtaining these spectra from Eqs. (16) and (17):

$$S_{AA}(f) = \frac{|Z_0' + 1|^2 S_{\Psi\Psi}}{4S^2[|W_1|^2\cos^2 kl + |W_2|^2 \sin^2 kl - \mathrm{Im}(W_2 W_1^*)\sin 2kl]}, \tag{19}$$

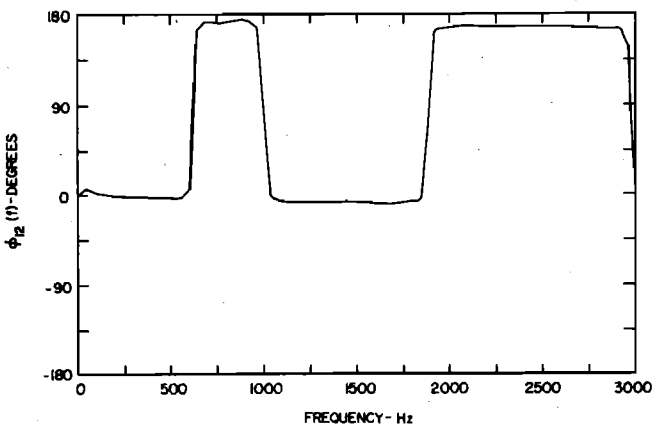

FIG. 6. Phase angle of the transfer function between first and second microphone for a closed tube.

$$S_{BB}(f) = \frac{|Z_0'-1|^2 S_{\psi\psi}}{4S^2[|W_1|^2\cos^2 kl + |W_2|^2\sin^2 kl - \mathrm{Im}(W_2W_1^*)\sin 2kl]}, \tag{20}$$

$$S_{AB}(f) = \frac{(|Z_0'|^2 - 2jY_0' - 1)S_{\psi\psi}}{4S^2[|W_1|^2\cos^2 kl + |W_2|^2\sin^2 kl - \mathrm{Im}(W_2W_1^*)\sin 2kl]}, \tag{21}$$

and combining Eqs. (19)–(21) with Eq. (18) yields

$$S_{11}(f) = \frac{[|Z_0'+1|^2 + |Z_0'-1|^2 + 2(|Z_0'|^2-1)\cos 2kx - 4Y_0'\sin 2kx]S_{\psi\psi}}{4S^2[|W_1|^2\cos^2 kl + |W_2|^2\sin^2 kl - \mathrm{Im}(W_2W_1^*)\sin 2kl]} = \frac{F_1(kx)}{F_2(kl)}, \tag{22}$$

where $W_1=(Z_i'+Z_0')$, $W_2=(Z_0'Z_i'+1)$, $Z_0'=R_0'+jY_0'$, $Z_i'=R_i'+jY_i'$, and $S_{\psi\psi}$ is the auto spectrum of $\psi(t)$.

An examination of Eqs. (19)–(21) shows that the auto- and cross-spectral densities are frequency dependent, even if the spectral density of the force is frequency independent.

The expected value of the estimate of $S_{11}(f)$ is defined by [9]

$$E[\hat{S}_{11}(f)] = \frac{1}{\Delta f}\int_{f-(\Delta f/2)}^{f+(\Delta f/2)} S_{11}(\xi)\,d\xi, \tag{23}$$

where $\hat{}$ denotes estimate and Δf is the analysis bandwidth. Combining Eqs. (22) and (23)

$$E[\hat{S}_{11}(f)] = \frac{1}{\Delta f}\int_{f-(\Delta f/2)}^{f+(\Delta f/2)} \frac{F_1(kx)}{F_2(kl)}\,df. \tag{24}$$

Suppose the force ψ is white noise with spectral density $S_{\psi\psi}=1$. Consider two cases of interest as follows:

Case 1: Provided Z_0' and Z_i' are constant and $x \ll l$, then $F_1(kx)$ is smoother than $F_2(kl)$ across the bandwidth Δf, and the integration in Eq. (24) can be carried out by assuming $F_1(kx) \approx$ constant. This yields (dropping the frequency dependency)

$$E[\hat{S}_{11}] = \frac{S_{11}(|W_1|^2\cos^2 kl + \mathrm{Im}(W_1W_2^*)\sin 2kl + |W_2|^2\sin^2 kl)}{S^2\{|W_1|^2|W_2|^2 - [\mathrm{Im}(W_1W_2^*)]^2\}^{1/2}}\left(\frac{1}{(2\pi\Delta f/c)l}\right)\left[\arctan\left(\frac{|W_2|^2\tan[(2\pi f/c)l + (\pi\Delta f/c)l] + \mathrm{Im}(W_1W_2^*)}{\{|W_1|^2|W_2|^2 - [\mathrm{Im}(W_1W_2^*)]^2\}^{1/2}}\right)\right.$$
$$\left. - \arctan\left(\frac{|W_2|^2\tan[(2\pi f/c)l - (\pi\Delta f/c)l] + \mathrm{Im}(W_1W_2^*)}{\{|W_1|^2|W_2|^2 - [\mathrm{Im}(W_1W_2^*)]^2\}^{1/2}}\right)\right]. \tag{25}$$

Equations (22) and (25) are plotted in Fig. 7 for several values of Δf for the case where $Z_i'=0.5+j.0.5$, $Z_0'=0.5+j.0.5$, $S=0.0079\ \mathrm{m}^2$, and $l=2$ m.

The bias error is defined as

$$b[\hat{S}_{11}] = E[\hat{S}_{11}] - S_{11}. \tag{26}$$

It can be seen from Fig. 7 that the largest bias error occurs at the peaks of the spectrum (i.e., at the tube resonances) which is consistent with the general result derived in Ref. 9. Inspection on Fig. 7 shows that a smaller error can be obtained by using a smaller bandwidth. However, a smaller bandwidth requires a larger amount of total data to maintain the same random error. [9]

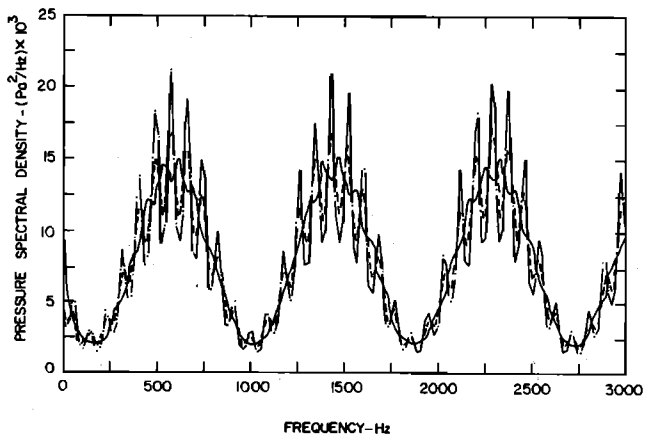

FIG. 7. Approximate calculation of the estimate $E[\hat{S}_{pp}]$ and the true value S_{pp} of the auto-spectral density function at $x=0.2$ m from the sample for several analysis bandwidths. Broken line: S_{pp}, dashed line: $E[\hat{S}_{pp}]$ for bandwidth=50 Hz. Solid line: $E[\hat{S}_{pp}]$ for bandwidth=100 Hz.

Case 2: If $F_2(kl)$ is smoother than $F_1(kx)$ across the bandwidth Δf and if Z_0' and Z_i' are constant, then Eq. (24) becomes

$$E[S_{11}(f)] = S_{AA}(f) + S_{BB}(f) + 2|S_{AB}(f)|\frac{\sin 2\pi x\Delta f/c}{2\pi x\Delta f/c}\cos(2kx-\theta), \tag{27}$$

where

$$\theta = \arctan[Q_{AB}(f)/C_{AB}(f)].$$

Equation (27) can be compared with the true spectral density given in Eq. (18). It is apparent from the third and fourth terms of Eq. (18) that a constant amplitude standing wave is present in the tube. Equation (27) shows that the amplitude of this standing wave decreases with x for Δf constant. Figure 8 contains a plot of Eq. (27) for the same set of parameters Z_0', Z_i', etc. used in case 1.

Equation (27) is an approximate result; the exact result is determined by numerical integration of Eq. (24) and is also shown in Fig. 8. The shift in the mean value of the curves in Fig. 8 is due to the bias error of $\hat{S}_{AA}(f)+\hat{S}_{BB}(f)$ which was neglected in the derivation of Eq. (27). The exact result also shows that the bias error of the standing wave ratio is greater than predicted by Eq. (27). The envelope of the true standing wave,

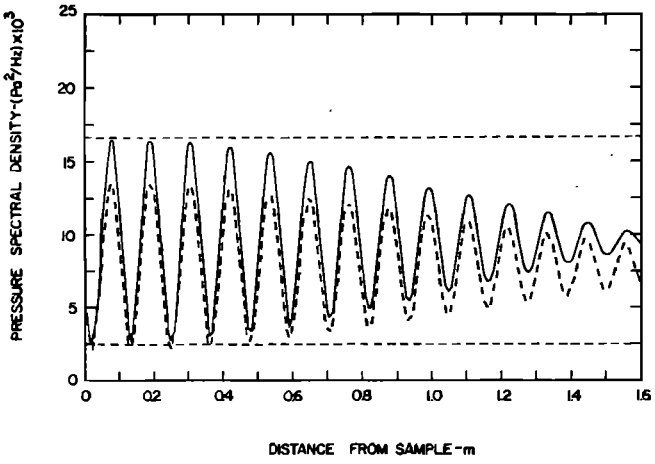

FIG. 8. Approximate and exact calculation of the auto-spectral density function estimate $E[\hat{S}_{pp}]$ versus distance from sample at 1500 Hz for $\Delta f = 100$ Hz. Dashed line: S_{pp}; dotted line: Exact $E[\hat{S}_{pp}]$; solid line: Approximate $E[\hat{S}_{pp}]$.

Eq. (18), is represented by the dashed lines in Fig. 8.

Figure 9 shows standing wave data obtained from an impedance tube in which the sample under study was a Helmholtz resonator with a resonant frequency of approximately 1000 Hz. These data clearly show the effect on standing wave ratio of increasing Δf and/or microphone position. The smallest bias error of $\hat{S}_{11}(f)$ will be obtained when Δf is small and the microphone is located close to the sample.

The bias error of $\hat{S}_{12}(f)$ may be found by examining $C_{12}(f)$ and $Q_{12}(f)$ separately, where $S_{12}(f) = C_{12}(f) + jQ_{12}(f)$. In Ref. 2 it is shown that

$$C_{12}(f) = [S_{AA}(f) + S_{BB}(f)]\cos k(x_1 - x_2) + 2[C_{AB}(f)\cos k(x_1 + x_2) + Q_{AB}(f)\sin k(x_1 + x_2)],$$

$$Q_{12}(f) = [-S_{AA}(f) + S_{BB}(f)]\sin k(x_1 - x_2).$$

Regarding the effect of the denominator on the bias error of $\hat{C}_{12}(f)$ and $\hat{Q}_{12}(f)$ (case 1), it is apparent that the behavior is similar to that described in Eq. (25). On the other hand, the numerator (case 2) introduces additional bias error in the estimates of $C_{12}(f)$ and

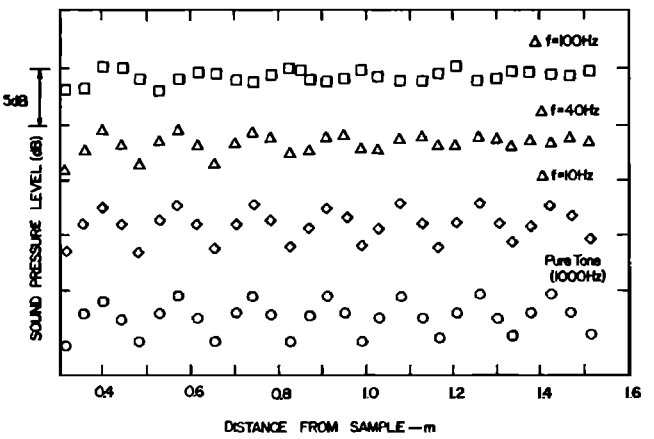

FIG. 9. Measured standing wave data showing the effect of bandwidth and distance from sample for a pure tone of 1000 Hz and for random noise filtered with various bandwidths centered at 1000 Hz.

$Q_{12}(f)$ as shown below:

$$E[\hat{C}_{12}(f)] = [S_{AA}(f) + S_{BB}(f)]\frac{\sin(\pi\Delta f/c)(x_1 - x_2)}{(\pi\Delta f/c)(x_1 - x_2)} \times \cos k(x_1 - x_2) + 2[C_{AB}(f)\cos k(x_1 + x_2) + Q_{AB}(f)\sin k(x_1 + x_2)]\frac{\sin(\pi\Delta f/c)(x_1 + x_2)}{(\pi\Delta f/c)(x_1 + x_2)},$$

$$E[\hat{Q}_{12}(f)] = [-S_{AA}(f) + S_{BB}(f)] \times \frac{\sin(\pi\Delta f/c)(x_1 - x_2)}{(\pi\Delta f/c)(x_1 - x_2)}\sin k(x_1 - x_2).$$

It can be seen from these equations that a smaller microphone spacing $(x_1 - x_2)$ yields a smaller bias error in $\hat{Q}_{12}(f)$ and also in the first two terms of $\hat{C}_{12}(f)$. The previous conclusions regarding the effect of Δf and microphone location on the bias error of $\hat{S}_{11}(f)$ also apply to $\hat{S}_{12}(f)$.

III. RANDOM ERRORS

It has been shown that for the measurement of absorption coefficient and impedance an estimate of the ratio $S_{12}(f)/S_{11}(f)$ is required. This ratio, or transfer function, can be represented as

$$H_{12}(f) = |H_{12}(f)|e^{j\phi_{12}(f)} = S_{12}(f)/S_{11}(f), \quad (28)$$

where $|H_{12}(f)|$ and $\phi_{12}(f)$ are the magnitude and phase angle, respectively, of the transfer function. To evaluate the random error, consider the two microphones and the tube as a bivariate linear process[10] as shown in Fig. 10. In Fig. 10, p_1 and p_2 are the acoustic pressures at points 1 and 2 in the tube, S_0 is the acoustic source used to excite a random sound field in the tube and N_0 represents any background noise sources that may be present. These sources are related to the acoustic pressures by the linear systems h_{1S}, h_{2S}, h_{1N}, and h_{2N}.

Using a Taylor series with a first order approximation, the variance of $|\hat{H}_{12}(f)|$ can be found by[11] (dropping f)

$$\mathrm{var}(|\hat{H}_{12}|) \approx \left(\frac{\partial|\hat{H}_{12}|}{\partial|\hat{S}_{12}|}\right)^2 \mathrm{var}(|\hat{S}_{12}|) + \left(\frac{\partial|\hat{H}_{12}|}{\partial\hat{S}_{11}}\right)^2 \times \mathrm{var}(\hat{S}_{11}) + 2\left(\frac{\partial|\hat{H}_{12}|}{\partial|\hat{S}_{12}|}\right)\left(\frac{\partial|\hat{H}_{12}|}{\partial\hat{S}_{11}}\right)\mathrm{cov}(|\hat{S}_{12}|, \hat{S}_{11}), \quad (29)$$

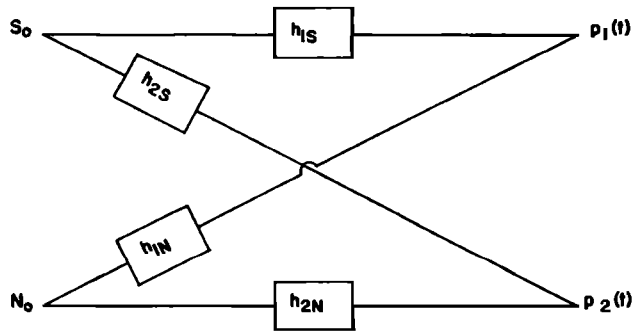

FIG. 10. Bivariate linear process describing the model of the tube and microphone system.

where the derivatives are determined from Eq. (28) and are evaluated at the true values, i.e., $E[|\hat{H}_{12}|]=|H_{12}|$, $E[|\hat{S}_{12}|]=|S_{12}|$ and $E[\hat{S}_{11}]=S_{11}$, assuming negligible bias errors. From Ref. 10

$$\mathrm{var}(|\hat{S}_{12}|)\approx(1/2n_d)|S_{12}|^2(1+1/\gamma_{12}^2), \tag{30}$$

and

$$\mathrm{var}(\hat{S}_{11})\approx(1/n_d)S_{11}^2. \tag{31}$$

The covariance

$$\mathrm{cov}(|\hat{S}_{12}|,\hat{S}_{11})\approx|S_{12}|S_{11}/n_d \tag{32}$$

is derived in the Appendix.

Using Eqs. (28)–(32)

$$\mathrm{var}(|\hat{H}_{12}|)\approx|H_{12}|^2(1/2n_d)[(1/\gamma_{12}^2)-1], \tag{33}$$

which is the same result obtained by Bendat[6] for a single input/output system with measurement interference at the output. The variance of $\hat{\phi}_{12}$ is[10]

$$\mathrm{var}(\hat{\phi}_{12})\approx(1/2n_d)[(1/\gamma_{12}^2)-1]. \tag{34}$$

In Eqs. (30)–(34) γ_{12}^2 is the coherence between the acoustic pressures and n_d is the number of raw spectral estimates used to compute the smooth spectral estimates $\hat{S}_{11}$ and $\hat{S}_{12}$.

A. The role of coherence

Equations (33) and (34) show that the variance on $|\hat{H}_{12}|$ or $\hat{\phi}_{12}$ depends on the coherence function between p_1 and p_2. The variance decreases as γ_{12}^2 approaches unity. The implication of high coherence may be seen by considering again the bivariate linear process in Fig. 10. Suppose S_0 and N_0 in Fig. 10 are uncorrelated white noise sources with zero mean:

$$p_1(t)=\int_0^\infty h_{1S}(u)S_0(t-u)du+\int_0^\infty h_{1N}(u)N_0(t-u)du, \tag{35}$$

$$p_2(t)=\int_0^\infty h_{2S}(v)S_0(t-v)dv+\int_0^\infty h_{2N}(v)N_0(t-v)dv. \tag{36}$$

The cross correlation $R_{12}(\tau)$ between $p_1(t)$ and $p_2(t)$ is

$$R_{12}(\tau)=E[p_1(t)p_2(t+\tau)]=\int_0^\infty\int_0^\infty h_{1S}(u)h_{2S}(v)\times E[S_0(t-u)S_0(t-v+\tau)]du\,dv+\int_0^\infty\int_0^\infty h_{1N}(u)h_{2N}(v)E[N_0(t-u)N_0(t-v+\tau)]du\,dv. \tag{37}$$

Since S_0 and N_0 are white noise processes,

$$E[S_0(t-u)S_0(t-v+\tau)]=R_{S_0}(\tau)=\sigma_S^2\delta(\tau+u-v), \tag{38}$$

$$E[N_0(t-u)N_0(t-v+\tau)]=R_{N_0}(\tau)=\sigma_N^2\delta(\tau+u-v), \tag{39}$$

where σ_S^2 and σ_N^2 are the variance of the source S_0 and background noise N_0, respectively. Combining Eqs. (37)–(39) yields

$$R_{12}(\tau)=\sigma_S^2\int_0^\infty h_{1S}(v-\tau)h_{2S}(v)dv+\sigma_N^2\int_0^\infty h_{1N}(v-\tau)h_{2N}(v)dv. \tag{40}$$

Setting $w=v-\tau$ and taking the Fourier transform of Eq. (40) gives

$$S_{12}(f)=\sigma_S^2H_{1S}^*(f)H_{2S}(f)+\sigma_N^2H_{1N}^*(f)H_{2N}(f), \tag{41}$$

where $H_{1S}(f)$, $H_{2S}(f)$, $H_{1N}(f)$, $H_{2N}(f)$ are the Fourier transforms of $h_{1S}(u)$, $h_{2S}(u)$, $h_{1N}(v)$, $h_{2N}(v)$, respectively, and $S_{12}(f)$ is the Fourier transform of $R_{12}(\tau)$.

Likewise the auto-spectral densities of $p_1(t)$ and $p_2(t)$ are

$$S_{11}(f)=\sigma_S^2|H_{1S}(f)|^2+\sigma_N^2|H_{1N}(f)|^2, \tag{42}$$

$$S_{22}(f)=\sigma_S^2|H_{2S}(f)|^2+\sigma_N^2|H_{2N}(f)|^2. \tag{43}$$

Using Eqs. (41), (42), and (43) and the definition of coherence function, $\gamma_{12}^2\equiv|S_{12}|^2/S_{11}S_{22}$:

$$\gamma_{12}^2=\frac{\sigma_S^4|H_{1S}|^2|H_{2S}|^2+2\sigma_S^2\sigma_N^2\mathrm{Re}(H_{1S}^*H_{2S}H_{1N}H_{2N}^*)+\sigma_N^4|H_{1N}|^2|H_{2N}|^2}{\sigma_S^4|H_{1S}|^2|H_{2S}|^2+\sigma_S^2\sigma_N^2(|H_{1S}|^2|H_{2N}|^2+|H_{1N}|^2|H_{2S}|^2)+\sigma_N^4|H_{1N}|^2|H_{2N}|^2}, \tag{44}$$

where the subscript f has been omitted for simplicity.

An examination of Eq. (44) shows that $\gamma_{12}^2=1$ when $\sigma_N^2=0$, when

$$H_{1S}=H_{1N}\ \text{ and }\ H_{2S}=H_{2N}, \tag{45}$$

or when

$$H_{1S}=H_{2S}\ \text{ and }\ H_{1N}=H_{2N}. \tag{46}$$

It is highly unlikely that Eq. (45) is fulfilled in practice since it implies that the sources coincide. Equation (46) implies the practical result that the coherence will be high if the microphone spacing is small.

B. Variance on $\hat{\alpha}_n$

The variance on $\hat{\alpha}_n$ can be found using Eq. (10) and the Taylor series approximation as used in Eq. (29):

$$\mathrm{var}(\hat{\alpha}_n)\approx\left(\frac{4\sin\phi_{12}\sin kL(|H_{12}|^2-1)}{(1+|H_{12}|^2-2|H_{12}|\cos\phi_{12}\cos kL-2|H_{12}|\sin\phi_{12}\sin kL)^2}\right)^2\mathrm{var}(|\hat{H}_{12}|)+\left(\frac{8|H_{12}|^2\sin kL\cos kL-4|H_{12}|\cos\phi_{12}\sin kL(|H_{12}|^2+1)}{(1+|H_{12}|^2-2|H_{12}|\cos\phi_{12}\cos kL-2|H_{12}|\sin\phi_{12}\sin kL)^2}\right)^2\mathrm{var}(\hat{\phi}_{12}), \tag{47}$$

where $\mathrm{cov}(|\hat{H}_{12}|,\hat{\phi}_{12})\approx0$ (see Appendix). Using Eqs. (33) and (34) in (47), the variance on $\hat{\alpha}_n$ can be expressed as

$$\mathrm{var}(\hat{\alpha}_n) \approx [G_1(|H_{12}|, \phi_{12}, kL) + G_2(|H_{12}|, \phi_{12}, kL)](1/\gamma_{12}^2 - 1)/2n_d, \tag{48}$$

where

$$G_1(|H_{12}|, \phi_{12}, kL) = \left(\frac{4|H_{12}|\sin\phi_{12}\sin kL(|H_{12}|^2 - 1)}{(1 + |H_{12}|^2 - 2|H_{12}|\cos\phi_{12}\cos kL - 2|H_{12}|\sin\phi_{12}\sin kL)^2}\right)^2, \tag{49}$$

and

$$G_2(|H_{12}|, \phi_{12}, kL) = \left(\frac{8|H_{12}|^2\sin kL\cos kL - 4|H_{12}|\cos\phi_{12}\sin kL(|H_{12}|^2 + 1)}{(1 + |H_{12}|^2 - 2|H_{12}|\cos\phi_{12}\cos kL - 2|H_{12}|\sin\phi_{12}\sin kL)^2}\right)^2, \tag{50}$$

are the error contribution functions of $|\hat{H}_{12}|$ and $\hat{\phi}_{12}$, respectively.

Equations (6) through (8) may be solved for α and β, and noting that $|H_{12}|^2 = \alpha^2 + \beta^2$ and $\phi_{12} = \arctan(\beta/\alpha)$:

$$|H_{12}|e^{j\phi_{12}} = \frac{e^{-jkx_2} + r_p e^{jkx_2}}{e^{-jkx_1} + r_p e^{jkx_1}}. \tag{51}$$

The error contribution functions may be calculated by specifying Z_0', x_2, and x_1 and by using Eqs. (6) and (51) with Eqs. (49) and (50).

Equations (32)–(34) and (47) reveal that the variance on α_n depends on the coherence function and the transfer function. The lowest coherence occurs at frequencies where either microphone coincides with a node of the standing wave (see Fig. 4). At these frequencies, the coherence is lowest when $R_0 \to 0$, $Y_0 \to \infty$. For this situation $|H_{12}| \to \infty$ or zero, and $\phi_{12} \to \pi/2$. Calculating G_1 and G_2 from Eqs. (49) and (50) and defining the normalized standard error $\epsilon_\alpha = [\mathrm{var}(\hat{\alpha}_n)]^{1/2}/\alpha_n$ yields

$$\epsilon_\alpha \approx [(1 - \gamma_{12}^2)/2n_d\gamma_{12}^2]^{1/2}. \tag{52}$$

Equation (52) shows that the error can be minimized by a high value of coherence and/or a high value of n_d. Since the coherence is generally high at other microphone positions and other frequencies, the role of the error contribution function G_1 and G_2 is usually insignificant. However, G_1 and G_2 are very large when $kL \to 0$ or $kL \to \pi$, and the normalized standard error $\epsilon_\alpha \to \infty$ when these conditions occur. For these frequencies α_n is not defined [see Eq. (10)]; therefore the measurement technique is restricted to $0 < kL < \pi$.

As an example of the variance on α_n consider a situation where $\gamma_{12}^2 = 0.5$ and $n_d = 50$. For this case Eq. (52) yields $\epsilon_\alpha = 0.1$, or 10%. Generally, however, less reflective materials will have lower normalized standard error because the coherence is approximately unity even at frequencies when the microphones coincide with nodes of the standing wave.

From Eqs. (7) and (8) the variance of the real and imaginary parts of the impedance can be derived using a Taylor series approximation as in the previous case for α_n. The results are straightforward but lengthy, and they are presented elsewhere.[12]

As an illustration of the error on the impedance calculation, consider, for example, the result of the measurement of a highly reflective material shown in Fig. 3. The corresponding transfer function is shown in Fig. 5. It is seen that a dip in the transfer function occurs at 1000 Hz, which corresponds to the frequency where the coherence is very low (see Fig. 4). This is the situation where a node coincides with the position of the first microphone. Although the variance on $|H_{12}|$ is very high at this frequency, the normalized standard error on the impedance for this sample is very small[12] which can be seen from the measurement result in comparison with the theoretical calculation shown in Fig. 3.

IV. SUMMARY AND CONCLUSIONS

Bias and random errors were derived for estimating the pressure spectral density of random sound fields in ducts. The major emphasis of this paper was the examination of how these errors affect the validity of acoustic property measurements. The bias errors were calculated using approximate and exact computation. To evaluate the random errors a bivariate linear process was employed to model the acoustic sources and the sound field. Experimental data were presented to verify the behavior of the bias and random errors. These data show good agreement with the theoretical analysis.

The bias errors of the pressure spectral density are a function of the microphone position and the analysis bandwidth used in the signal processing. It was shown that the standing wave of the pressure spectral density in a small frequency band decreases with distance from the end of the duct. It turns out that the bias errors can be reduced by locating the microphone close to the sample and/or by selecting a small analysis bandwidth.

The random errors, on the other hand, can be minimized by maintaining a high coherence between the acoustic source and the pressure in the duct. The higher coherence can be achieved by minimizing noise sources and by choosing a smaller microphone spacing. However, a smaller microphone spacing will reduce the accuracy of the measurements at low frequency because of the large error when $kL \to 0$. A large error also occurs when $kL \to \pi$, corresponding to a microphone spacing of $\lambda/2$, and when a node coincides with a microphone position.

The constraints mentioned above are not normally severe and can usually be accommodated. The data in this paper and in Refs. 2 and 3 show that acoustic properties may be determined with good accuracy when random excitation is used, providing proper attention is given to signal processing requirements.

ACKNOWLEDGMENT

The authors are grateful to IBM, Office Products Division, Lexington, Kentucky, for providing experi-

mental facilities for obtaining standing wave data.

APPENDIX

A. Derivation of $\mathrm{cov}(|\hat{S}_{12}|, \hat{S}_{11})$

Consider the estimate of the cross-spectral density

$$\hat{S}_{12} = \hat{C}_{12} + j\hat{Q}_{12}, \tag{A1}$$

where $\hat{C}_{12}$ and $\hat{Q}_{12}$ are the real and imaginary parts of $\hat{S}_{12}$, respectively. It follows that

$$|\hat{S}_{12}| = (\hat{C}_{12}^2 + \hat{Q}_{12}^2)^{1/2}. \tag{A2}$$

Writing in the perturbation form,

$$\hat{C}_{12} = C_{12} + \delta\hat{C}_{12}, \quad \hat{Q}_{12} = Q_{12} + \delta\hat{Q}_{12}, \tag{A3}$$

$$\hat{S}_{11} = S_{11} + \delta\hat{S}_{11}, \tag{A4}$$

$$E[\delta\hat{C}_{12}] = 0, \quad E[\delta\hat{Q}_{12}] = 0, \quad E[\delta\hat{S}_{11}] = 0,$$

$$E[\delta\hat{C}_{12}\delta\hat{S}_{11}] = \mathrm{cov}(\hat{C}_{12}, \hat{S}_{11}),$$

$$E[\delta\hat{Q}_{12}\delta\hat{S}_{11}] = \mathrm{cov}(\hat{Q}_{12}, \hat{S}_{11}), \tag{A5}$$

Eq. (A2) becomes

$$|\hat{S}_{12}| = [(C_{12} + \delta\hat{C}_{12})^2 + (Q_{12} + \delta\hat{Q}_{12})^2]^{1/2}, \tag{A6}$$

which, by using a Taylor series approximation around the true value, yields

$$|\hat{S}_{12}| \approx |S_{12}|\left(1 + \frac{C_{12}\delta\hat{C}_{12} + Q_{12}\delta\hat{Q}_{12}}{|S_{12}|^2}\right). \tag{A7}$$

Multiplying Eqs. (A4) and (A7)

$$|\hat{S}_{12}|\hat{S}_{11} \approx |S_{12}|S_{11} + \frac{(C_{12}\delta\hat{C}_{12} + Q_{12}\delta\hat{Q}_{12})}{|S_{12}|}S_{11} + |S_{12}|\delta\hat{S}_{11} + \frac{C_{12}\delta\hat{C}_{12}\delta\hat{S}_{11} + Q_{12}\delta\hat{Q}_{12}\delta\hat{S}_{11}}{|S_{12}|},$$

and taking expected values

$$E[|\hat{S}_{12}|\hat{S}_{11}] \approx |S_{12}|S_{11} + \frac{C_{12}S_{11}}{|S_{12}|}E[\delta\hat{C}_{12}] + \frac{Q_{12}S_{11}}{|S_{12}|}E[\delta\hat{Q}_{12}] + |S_{12}|E[\delta\hat{S}_{11}] + \frac{C_{12}\,\mathrm{cov}(\hat{C}_{12}, \hat{S}_{11})}{|S_{12}|} + \frac{Q_{12}\,\mathrm{cov}(\hat{Q}_{12}, \hat{S}_{11})}{|S_{12}|}. \tag{A8}$$

From Ref. 10:

$$\mathrm{cov}(\hat{C}_{12}, \hat{S}_{11}) \approx C_{12}S_{11}/n_d, \tag{A9}$$

$$\mathrm{cov}(\hat{Q}_{12}, \hat{S}_{11}) \approx Q_{12}S_{11}/n_d. \tag{A10}$$

Using Eqs. (A5), (A9), and (A10) in (A8) yields

$$E[|\hat{S}_{12}|\hat{S}_{11}] \approx |S_{12}|S_{11} + |S_{12}|S_{11}/n_d. \tag{A11}$$

From the definition of covariance

$$\mathrm{cov}(|\hat{S}_{12}|, \hat{S}_{11}) = E[(|\hat{S}_{12}| - |S_{12}|)(\hat{S}_{11} - S_{11})] = E[|\hat{S}_{12}|\hat{S}_{11}] - |S_{12}|S_{11}. \tag{A12}$$

Using Eq. (A11) in Eq. (A12)

$$\mathrm{cov}(|\hat{S}_{12}|\hat{S}_{11}) \approx |S_{12}|S_{11}/n_d. \tag{A13}$$

B. Derivation of $\mathrm{cov}(|\hat{H}_{12}|, \hat{\phi}_{12})$

The estimate of the transfer function is defined by

$$\hat{H}_{12} = \hat{S}_{12}/\hat{S}_{11}, \tag{A14}$$

$$|\hat{H}_{12}| = |\hat{S}_{12}|/\hat{S}_{11}, \tag{A15}$$

$$\hat{\phi}_{12} = \arctan(\hat{Q}_{12}/\hat{C}_{12}). \tag{A16}$$

Expanding Eqs. (A15) and (A16) in a Taylor series around the true value yields, to a first order approximation,

$$|\hat{H}_{12}| \approx |H_{12}| + \frac{\delta|\hat{S}_{12}|}{S_{11}} - \frac{S_{12}\delta\hat{S}_{11}}{S_{11}^2}, \tag{A17}$$

$$\hat{\phi}_{12} \approx \phi_{12} + \frac{C_{12}\delta\hat{Q}_{12}}{|S_{12}|^2} - \frac{Q_{12}\delta\hat{C}_{12}}{|S_{12}|^2}. \tag{A18}$$

Using Eqs. (A17) and (A18),

$$E[|\hat{H}_{12}|\hat{\phi}_{12}] \approx |H_{12}|\phi_{12} + \frac{C_{12}}{S_{11}|S_{12}|^2}\mathrm{cov}(|\hat{S}_{12}|, \hat{Q}_{12}) - \frac{Q_{12}}{|S_{12}|^2S_{11}}\mathrm{cov}(|\hat{S}_{12}|, \hat{C}_{12}) - \frac{C_{12}}{|S_{12}|S_{11}^2}\mathrm{cov}(\hat{S}_{11}, \hat{Q}_{12}) + \frac{Q_{12}}{|S_{12}|S_{11}^2}\mathrm{cov}(\hat{S}_{11}, \hat{C}_{12}). \tag{A19}$$

By substituting $\hat{Q}_{12} = |\hat{S}_{12}|\sin\hat{\phi}_{12}$ and $\hat{C}_{12} = |\hat{S}_{12}|\cos\hat{\phi}_{12}$, and using a Taylor series expansion around the true value for $\sin\hat{\phi}_{12}$ and $\cos\hat{\phi}_{12}$, it can be shown that

$$\mathrm{cov}(|\hat{S}_{12}|, \hat{Q}_{12}) \approx -\sin\phi_{12}\,\mathrm{var}(|\hat{S}_{12}|), \tag{A20}$$

$$\mathrm{cov}(|\hat{S}_{12}|, \hat{C}_{12}) \approx -\cos\phi_{12}\,\mathrm{var}(|\hat{S}_{12}|). \tag{A21}$$

Employing Eqs. (A9), (A10), (A20), and (A21) in (A19) yields

$$E[|\hat{H}_{12}|\hat{\phi}_{12}] \approx |H_{12}|\phi_{12}. \tag{A22}$$

Hence

$$\mathrm{cov}(|\hat{H}_{12}|, \hat{\phi}_{12}) = E[(|\hat{H}_{12}| - |H_{12}|)(\hat{\phi}_{12} - \phi_{12})] = E[|\hat{H}_{12}|\hat{\phi}_{12}] - |H_{12}|\phi_{12} \approx 0. \tag{A23}$$

[1] J. P. Johnston and W. E. Schmidt, "Measurement of acoustic reflection from an obstruction in a pipe with flow," J. Acoust. Soc. Am. 63 (5), 1455–1460 (1978).

[2] A. F. Seybert and D. F. Ross, "Experimental determination of acoustic properties using a two-microphone random-excitation technique," J. Acoust. Soc. Am. 61 (5), 1362–1370 (1977).

[3] J. Y. Chung and D. A. Blaser, "Transfer function method of measuring in-duct acoustic properties. I. Theory, II. Experiment," J. Acoust. Soc. Am. 68 (3), 907–921 (1980).

[4] T. L. Parrott and C. D. Smith, "Random and systematic measurement errors in acoustic impedance as determined by the transmission line method," NASA Technical Note TN D-8520 (December 1977).

[5] B. D. Rapp, "A two-microphone method for evaluating the normal incidence properties of acoustical systems and materials," Master's thesis, Mech. Engr. Dept., University of Kentucky (1978).

[6] J. S. Bendat, "Statistical errors in measurement of coherence functions and input/output quantities," J. Sound Vib. 59, 405–421 (1978).

[7]I. Dyer, "Measurement of noise sources in ducts," J. Acoust. Soc. Am. 30, 833–841 (1958).
[8]The plane wave, however, may be maintained without being contaminated with higher order modes, regardless of the diameter of the tube, if the source is an ideal flat or perfect piston [see P. M. Morse and K. Uno Ingard, *Theoretical Acoustics* (McGraw–Hill, New York, 1968)].
[9]J. S. Bendat and A. G. Piersol, *Random Data: Analysis and Measurement Procedures* (Wiley Interscience, New York, 1971).
[10]G. M. Jenkins and D. G. Watts, *Spectral Analysis and its Applications* (Holden–Day, San Francisco, 1968).
[11]A. Papoulis, *Probability, Random Variables, and Stochastic Processes* (McGraw–Hill, New York, 1965).
[12]B. Soenarko, "Error analysis of spectral estimates with application to the measurement of acoustic parameters using random sound fields in ducts," Master's thesis, Mech. Engr. Dept., University of Kentucky (1980).